Journal of Integrative Neuroscience

J. Integr. Neurosci. **2026**; 25(6): 48602
https://doi.org/10.31083/JIN48602

Original Research

High-Frequency Repetitive Transcranial Magnetic Stimulation Improves Oxidative Stress, Iron Metabolism, and Synaptic Plasticity in the Visual Cortex of Amblyopic Rats: Association With the NRF2/GPX4 Pathway

Qin Li[1,2,3], Yinyin You[1,2,3], Qing Lu[1,2,3], Yunchun Zou[1,2,3,*], Xiong Yang[2], Haorong Wang[2], Wenchuan Liao[2], Zhe Li[2], Lingjun Wei[4], Weiqi Song[4]

[1]Department of Ophthalmology, The Second Clinical College of North Sichuan Medical College (Nanchong Central Hospital), 637000 Nanchong, Sichuan, China
[2]Department of Optometry, North Sichuan Medical College, 637000 Nanchong, Sichuan, China
[3]Department of Ophthalmology, Eye Hospital of Nanchong, 637000 Nanchong, Sichuan, China
[4]Department of Optometry, Zhoukou Central Hospital, 466000 Zhoukou, Henan, China
*Correspondence: zychun03@163.com (Yunchun Zou)
Academic Editor: Bettina Platt
Submitted: 27 November 2025 Revised: 27 February 2026 Accepted: 12 March 2026 Published: 26 June 2026

Abstract

Background: Amblyopia is a neurodevelopmental disorder with limited treatment efficacy after the developmental critical period. Repetitive transcranial magnetic stimulation (rTMS) improves visual perception in patients with amblyopia, although its specific mechanism remains unclear. In this study, we investigated whether rTMS improves abnormal ocular dominance (OD) distribution in monocular deprivation (MD) amblyopic rats by modulating oxidative stress, iron metabolism, and synaptic plasticity through the nuclear factor erythroid 2-related factor 2/glutathione peroxidase-4 (NRF2/GPX4) pathway. **Methods**: Sprague-Dawley (SD) rats were randomly assigned to four groups (n = 20 each): normal control+rTMS (NC+rTMS), NC+sham stimulation (NC+sham), MD+sham, and MD+rTMS. The rTMS groups received 20-Hz rTMS treatment for 28 consecutive days. Visual function was assessed using flash visual evoked potentials (F-VEP). The morphological structure of the visual cortex, synaptic function, oxidative stress levels, iron metabolism, and expression of NRF2/GPX4 were analyzed using histopathological staining, transmission electron microscopy (TEM), biochemical assay, and molecular biology experiments. Statistical analyses were performed using repeated-measures analysis of variance (ANOVA) and two-way ANOVA. Bonferroni post-hoc tests were used afterward. **Results**: Following rTMS treatment, the contralateral vs. ipsilateral value (C/I values) in the MD+rTMS group were higher than baseline ($p < 0.0001$). Compared with the MD+sham group, rTMS alleviated visual cortex synaptic ultrastructural damage and upregulated postsynaptic density protein 95 (PSD-95) and brain-derived neurotrophic factor (BDNF) levels in MD rats ($p = 0.016$, $p = 0.041$). The MD+rTMS group showed significantly decreased reactive oxygen species (ROS) and malondialdehyde (MDA) levels ($p < 0.05$, $p < 0.0001$) and increased glutathione (GSH) content ($p < 0.0001$) in comparison with the MD+sham group. Additionally, rTMS elevated NRF2, GPX4, and ferroportin-1 (FPN1) expression in the MD group (all $p < 0.01$) and reduced ferrous iron (Fe^{2+}) accumulation ($p < 0.01$) relative to the MD+sham group. **Conclusions**: High-frequency rTMS improves abnormal OD distribution in amblyopic rats, an effect associated with the upregulation of NRF2/GPX4 pathway protein expression, reduced oxidative stress, restored iron metabolism, and enhanced synaptic plasticity in the visual cortex. This finding offers novel insights into the mechanisms of rTMS and the pathology of amblyopia.

Keywords: amblyopia; repetitive transcranial magnetic stimulation; nuclear factor erythroid 2-related factor 2/glutathione peroxidase-4; synaptic plasticity; iron metabolism

1. Introduction

Amblyopia is a frequent visual disorder during the critical developmental period in children. It is closely associated with impaired structural and functional plasticity in the visual cortex [1]. Epidemiological data indicate a global prevalence of 1.36% for amblyopia, with 1.09% in Asia [2]. Amblyopic patients often exhibit not only reduced visual acuity but also deficits in stereopsis, spatial orientation, and contrast sensitivity [3]. Despite common interventions such as occlusion therapy and refractive correction, outcomes remain suboptimal for some patients, particularly after the critical period when therapeutic efficacy significantly declines [4]. Thus, exploring new approaches that reactivate cortical plasticity and improve visual function remains a priority.

Repetitive transcranial magnetic stimulation (rTMS) is a non-invasive neuromodulation technique capable of modulating cortical excitability and inducing neural plasticity [5]. Previous studies have demonstrated that either high (10 Hz) or low (1 Hz) frequency rTMS enhances synaptic

Copyright: © 2026 The Author(s). Published by IMR Press.
This is an open access article under the CC BY 4.0 license.

Publisher's Note: IMR Press stays neutral with regard to jurisdictional claims in published maps and institutional affiliations.

plasticity in the visual cortex. They also promote neural network remodeling and ameliorate impairments in visual acuity, contrast sensitivity, and stereopsis in amblyopic patients [6,7]. However, the specific mechanisms remain to be fully elucidated.

Nuclear factor erythroid 2-related factor 2 (NRF2) is a crucial transcription factor that activates antioxidant and cytoprotective responses [8]. Previous studies have demonstrated that NRF2 participates in regulating mitochondrial energy metabolism in visual cortex neurons, playing a key role in plasticity in the visual cortex [9,10]. However, NRF2 deficiency leads to iron overload and lipid peroxidation accumulation, subsequently impairing synaptic plasticity and functional connectivity in the brain [11]. Glutathione peroxidase-4 (GPX4), an antioxidant enzyme that effectively suppresses lipid peroxidation and prevents ferroptosis, has its activity regulated by NRF2 [12]. The NRF2/GPX4 pathway has been demonstrated to play a crucial role in various neurological disorders [13,14]. However, its role in amblyopia remains less understood. As the most plentiful trace element in the human body, iron participates in multiple physiological processes, and its metabolic balance is crucial for neural development and functional maintenance [15]. Further, disordered iron metabolism may induce ferroptosis—a distinct type of cell death marked with iron overload and lipid oxidative damage [16]. Recent studies indicate that high-frequency rTMS activates the NRF2/GPX4 pathway in the hippocampus, thereby reducing oxidative stress, counteracting ferroptosis, and improving cognitive dysfunction [17,18]. However, it remains unclear whether the therapeutic effect of high-frequency rTMS on amblyopia is exerted by the regulation of the NRF2/GPX4 pathway in the visual cortex.

Therefore, this study aims to establish a monocular deprivation (MD) amblyopic rat model to analyze proteins associated with the NRF2/GPX4 pathway, thus investigating the effects of rTMS intervention on neural plasticity, oxidative stress, and iron metabolism in the visual cortex of amblyopic rats. A further aim is to contribute fresh theoretical foundations to guide the clinical application of rTMS, and through this, open new ways to understand the pathogenesis of amblyopia.

2. Materials and Methods

2.1 Materials

Experimental Animals and Grouping

This study utilized 80 three-week-old male SD rats as experimental subjects with an initial body weight of 45 ± 5 g. All rats underwent routine ocular examinations to exclude organic ocular lesions. Using a random number table, rats were divided into four groups: normal control+rTMS (NC+rTMS), NC+sham stimulation (NC+sham), monocular deprivation + sham stimulation (MD+sham), and MD+rTMS. Each group contained 20 rats. Animals were provided by the Animal Experiment Center of North Sichuan Medical College. Rats were housed in a facility under a 12-hour light-dark cycle, with a temperature maintained at 24 ± 1 °C and a relative humidity of 50%. Food and water were available ad libitum. The experimental arrangement of this study is given in Fig. 1.

2.2 Methods

2.2.1 Establishment of Animal Amblyopia Model

A classic amblyopia model was established by using MD. First, rats were anesthetized and immobilized with 1.25% Avertin (10 mL/kg, DW3120, Dowobio Biotechnology, Shanghai, China), the hair surrounding the right eyelid was shaved, and the adjacent skin was disinfected with povidone-iodine (HY-B2234, MedChemExpress, Shanghai, China). Subsequently, approximately 0.5–1.5 mm of tissue from the upper and lower eyelid margins was excised and intermittently sutured using 6-0 absorbable sutures. After suturing, ofloxacin eye ointment (H10940177, Xingqi Pharmaceutical, Shenyang, Liaoning, China) was applied to the wound site to prevent infection, and healing was monitored regularly. Throughout the MD modeling period, animals exhibiting suture dislodgement, or intraocular infection were excluded. As controls, rats in the NC+sham/rTMS group underwent identical anesthesia and margin trimming procedures without suturing.

2.2.2 rTMS Protocol

The rTMS stimulation was performed with a magnetic stimulator equipped with a butterfly coil (MCF-B65, outer diameter 80 mm, K071821, Medtronic, Copenhagen, Denmark) [19]. At the onset of rTMS intervention, following previous methods [6,20], a soft towel was used to gently wrap the rat's body, while its head was stabilized by supporting the cheek. The center of the coil was positioned over the scalp region, approximating the primary visual cortex (bregma coordinates approximately –6.0 to –8.0 mm posterior, midline) [21], with the coil plane held tangential to the head surface. Stimulation parameters were set as follows: frequency 20 Hz, stimulation 10 s, inter-stimulus interval 60 s, 30% maximum output intensity. Each daily session consisted of five stimulation trains, delivering a total of 1000 pulses per session. Stimulation was administered in weekly cycles of five consecutive days followed by two days of rest, repeated for a total of 28 consecutive calendar days. For the sham-stimulated rats, the coil was positioned 15 cm away from the head.

2.2.3 F-VEP Assessment

F-VEP was recorded in all groups before and after rTMS intervention by a visual electrophysiology system (RetiMINER IV, IRC Medical Equipment, Chongqing, China). The experimental setup and parameters were based on the principles of the International Society for Clinical Electrophysiology of Vision and optimized for use in rodents. The specific procedure was as follows: Rats

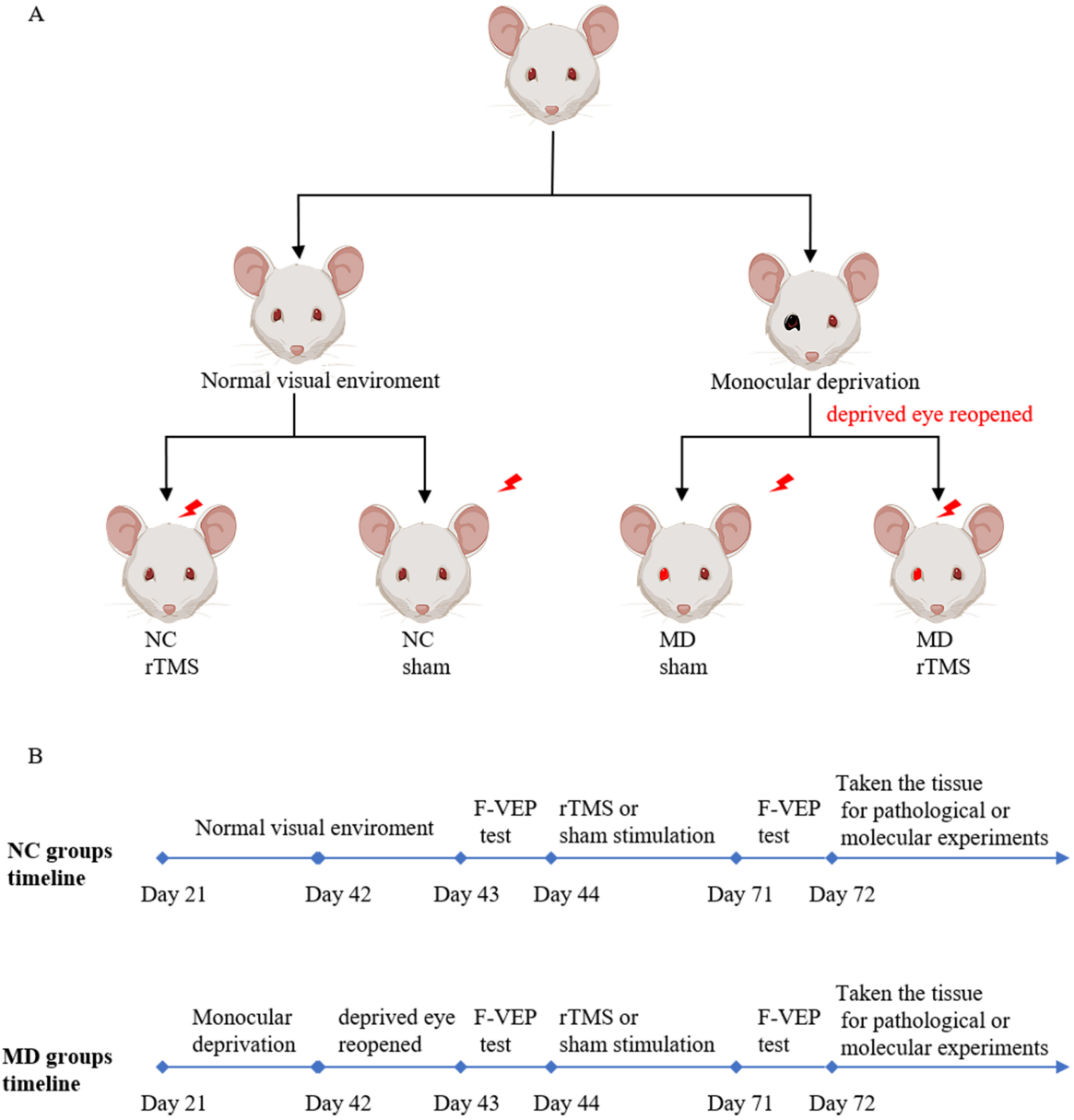

Fig. 1. Experimental grouping and procedure flow diagram of this study. (A) Experimental animal groups. (B) Timeline of related experiments for each group. MD, monocular deprivation; NC, normal control; rTMS, repetitive transcranial magnetic stimulation; F-VEP, flash visual evoked potentials.

were first dark-adapted for 12 hours, then anesthetized via intraperitoneal injection of 1.25% Avertin (10 mL/kg, DW3120, Dowobio Biotechnology). Compound tropicamide eye drops (H20055546, Xingqi Pharmaceutical, shenyang, liaoning, China) were then administered for complete mydriasis. Anesthetized rats were secured to the electrophysiology testing platform (RetiMINER IV, IRC Medical Equipment, Chongqing, China) and electrodes placed according to a previous study [6], with the recording electrode placed beneath the occipital scalp, the reference electrode positioned in the oral cavity, and the ground electrode implanted subcutaneously in the tail. F-VEP testing parameters were set as follows: Flicker light stimulation at 1 Hz frequency, 3.0 cd/m^2 intensity, 1–100 Hz bandpass filtering, and 100 signal superimpositions. During testing, the non-tested eye was covered with an opaque cloth. The amplitude of the P1 wave in the F-VEP waveform of each rat was recorded and the OD index (C/I) was calculated based on the formula [22]: C/I = amplitude of the contralateral eye/amplitude of the ipsilateral eye (contralateral eye: Deprived eye in the MD group or right eye in the NC group; ipsilateral eye: Non-deprived eye in the MD group or left eye in the NC group).

2.2.4 Nissl Staining

After completion of F-VEP testing, four rats were arbitrarily chosen from each group for the preparation of paraffin sections of the left visual cortex (the contralateral cortex to the deprived eye in MD rats or the contralateral cortex to the right eye in control rats) for Nissl and enhanced Prussian blue iron staining. Sections underwent routine xylene (25168-04-1, Denuo Chemical, Shanghai, China) dewaxing and graded ethanol rehydration, followed by rinsing with distilled water. They were then immersed in 0.1% Nissl (G1432, Solarbio, Beijing, China) solution for 10–15 min according to kit instructions. After staining, sections were washed with distilled water, dehydrated using graded ethanol and clarified using xylene. They were then coverslipped with neutral resin (G8590, Solarbio, Beijing, China) and allowed to dry for subsequent use. Neuronal morphology in the left primary visual cortex (V1) was observed under an optical microscope (Olympus DP74, Olympus Corporation, Tokyo, Japan). Four random fields of view (×400) were captured per section, and Nissl-positive cells in each field were counted using ImageJ software (ImageJ 1.54, National Institutes of Health, Bethesda, MD, USA). Statistical analysis was performed using the average value per animal.

2.2.5 Enhanced Prussian Blue Iron Staining

After dewaxing and rehydration, sections were dark incubated in Prussian blue (G1428, Solarbio, Beijing, China) solution for 30 minutes. Following staining, sections were rinsed with distilled water and stained with 3,3′-Diaminobenzidine (DAB) (DA1010, Solarbio, Beijing, China) solution for 10 minutes, with color development controlled under microscope observation. Sections were then rinsed again with distilled water, counterstained with hematoxylin (G1080, Solarbio, Beijing, China) for two minutes, dehydrated, cleared, and mounted following standard procedures. Iron distribution in the left V1 was observed under a light microscope, where iron-containing tissue areas appeared brownish.

2.2.6 Transmission Electron Microscopy (TEM)

A further four rats were randomly selected from each group. After deep anesthesia with Avertin (1.25%, 10 mL/kg), the rats were rapidly decapitated for euthanasia. The left visual cortex tissue was immediately excised and sectioned into approximately 1 mm^3 pieces. These were immediately fixed with 2.5% glutaraldehyde (111-30-8, Macklin Biochemical, Shanghai, China) and kept at 4 °C for 24 hours. Following osmium tetroxide (208868, Sigma-Aldrich Corporation, St. Louis, MO, USA) fixation, acetone (AX0120T, Sigma-Aldrich Corporation) dehydration, and epoxy resin (CY-10123, Delf Biotechnology, Hefei, Anhui, China) embedding, sections 70–90 nm thick were prepared. These were mounted on copper grids (930261, Sigma-Aldrich Corporation), then stained with uranyl acetate (541-09-3, Dideu New Materials Corporation, Yulin, Shaanxi, China) and lead citrate (HD17800, Hede biotechnology, Beijing, China). The synaptic ultrastructure of the left V1 was observed under a TEM (JEM-1400Flash, JEOL, Tokyo, Japan). Four randomly selected fields (×10,000) were photographed to analyze the parameters of synaptic structure using ImageJ, with statistical analysis performed based on the mean values per animal.

2.2.7 Dihydroethidium (DHE) Staining

Four rats per group were randomly euthanized. Freshly left visual cortex tissue was obtained with an optimal cutting temperature compound, embedded, and sectioned into frozen slices. These slices were then dark incubated at room temperature with the DHE fluorescent (GC30025, GlpbioTechnology LLC, Montclair, CA, USA) probe for 30 min. Cell nuclei were counterstained with 4′,6-diamidino-2-phenylindole (DAPI) (G1012, Servicebio, Wuhan, Hubei, China), washed with phosphate-buffered saline (PBS), and mounted. reactive oxygen species (ROS) staining in the left V1 was visualized with an upright fluorescence microscope (Olympus BX63, Olympus Corporation, Tokyo, Japan), with four non-overlapping fields (×400) randomly selected. Fluorescence intensity was subsequently measured using ImageJ software. DAPI-stained nuclei appeared blue, while fluorescently labeled positive cells appeared red.

2.2.8 Determination of MDA, GSH, and Fe^{2+} Content

Four rats in each group were sacrificed. The left visual cortex tissues were harvested and saved at –80 °C for biochemical assays. Portions of frozen tissue were washed in pre-chilled PBS, homogenized with extraction buffer, and centrifuged to collect supernatant. Total protein concentration was determined with the BCA Kit (ZJ101, Epizyme, Shanghai, China). Subsequently, MDA, GSH, and Fe^{2+} detection systems were added according to the kit instructions (E-BC-K025-M, E-BC-K030-M, E-BC-K773-M, Elabscience, Wuhan, Hubei, China). Absorbance was read at specific wavelengths with a microplate reader (Spectra Max Paradigm TUNE, Molecular Devices, Shanghai, China): MDA at 532 nm, GSH at 405 nm, and Fe^{2+} at 593 nm. The measured data were then substituted into their respective standard curve equations to calculate the content of each indicator and analyze its changes. The equations were: MDA: $Y = 0.0044_X + 0.0093$; GSH: $Y = 0.0067_X + 0.0142$; Fe^{2+}: $Y = 0.016_X + 0.0062$.

2.2.9 Western Blotting

The remaining four rats in each group were sacrificed. The left visual cortex tissues were harvested and stored at –80 °C for molecular biological assays. Subsequently, portions of the tissue samples were taken for protein extraction. Total protein concentration was determined using the BCA method. Based on the results, the

required volume for achieving a 40 µg loading amount in each group was calculated, and equivalent protein samples were added to the loading buffer for denaturation. 10% and 12.5% SDS-PAGE gels (PG112, PG113, Epizyme, Shanghai, China) were prepared based on the target protein molecular weights. Marker and protein samples were added for electrophoresis separation. Following electrophoresis, proteins were electrotransferred to polyvinylidene difluoride membranes (IPVH00010, Millipore, Burlington, MA, USA) and soaked in 5% skimmed milk at ambient temperature for two hours. Membranes were then washed in PBS with Tween-20 (PBST).

The following primary antibodies were subsequently added: PSD-95 (1:10,000, ET1602-20, HuaBio, Hangzhou, Zhejiang, China), BDNF (1:2000, HA722912, HuaBio), NRF2 (1:1000, YP-mAb-01916, UpingBio, Hangzhou, Zhejiang, China), GPX4 (1:1000, ET1706-45), FPN1 (1:1000, YP-mAb-17948, UpingBio), glyceraldehyde-3-phosphate dehydrogenase (GAPDH) (1:5000, R380626, Zenbio, Chengdu, Sichuan, China), and β-actin (1:5000, AB-2839420, Affinity, Changzhou, Jiangsu, China), and incubated at 4 °C for the night. The membranes were washed with PBST the next day. Species-specific secondary antibodies (goat anti-rabbit/anti-mouse, SA00001-2, SA00001-1, 1:5000, Proteintech, Wuhan, Hubei, China) were added and incubated at room temperature for one hour. After washing, the membranes were developed using an ECL chemiluminescent kit (BL520A, Biosharp, Beijing, China). Band intensity values were determined using ImageJ, with either GAPDH or β-actin as internal controls to calculate the relative expression levels of target proteins.

2.2.10 Quantitative RT-PCR (qRT-PCR)

Frozen brain tissues were extracted and placed in RNase EP-free tubes. Total RNA was extracted following the RNA extraction kit (5100050, Simgen, Hangzhou, Zhejiang, China) protocol and reversed transcribed into cDNA. mRNA levels of *PSD-95*, *BDNF*, *NRF2*, *GPX4*, *FPN1*, *GAPDH*, and *β-actin* genes in the visual cortex of rats were then detected across all groups using a RT-qPCR kit (Q711-02, Vazyme, Nanjing, Jiangsu, China). The reaction program was set as follows: 95 °C pre-denaturation for 30 s, followed by 40 cycles of denaturation at 95 °C for 5 s, annealing at 55 °C for 30 s, and extension at 72 °C for 30 s. After the reaction, the Ct values for each target gene and the internal control gene were collected. The relative mRNA content of the target genes was calculated using the $2^{-\Delta\Delta CT}$ method. The gene primers were designed and obtained from Sangon Biotech (Shanghai, China), and detailed sequences are given in Table 1.

2.3 Statistical Analysis

Data processing and statistical analyses were employed using IBM SPSS Statistics software (version 22.0, IBM Corporation, Armonk, NY, USA). A p value < 0.05 was considered statistically significant. GraphPad Prism 10.6.0 software (GraphPad Software, San Diego, CA, USA) was used for data visualization. Before formal analysis, the Shapiro-Wilk test was used to assess data normality. Quantitative results were expressed as the mean $\pm$ standard deviation (mean $\pm$ SD). ANOVA was applied to compare F-VEP outcomes obtained before and after rTMS intervention. Two-way ANOVA was used to compare the quantitative histological data (Nissl-positive cell count, synaptic-related structure indices, ROS fluorescence intensity) and molecular biological indicators (biochemical analysis, Western blotting, qRT-PCR). Post-hoc pairwise comparisons were conducted using Bonferroni tests.

3. Results

3.1 High-Frequency rTMS Affects Abnormal Ocular Dominance Distribution and Neuronal Function in MD Rats

To determine whether rTMS can ameliorate the abnormal ocular dominance (OD) in MD rats, F-VEPs were recorded pre- and post-intervention (Fig. 2A). Repeated-measures ANOVA of C/I values showed significant main effects of time [$F(1,76) = 49.833$, $p < 0.0001$] and treatment [$F(3,76) = 38.315$, $p < 0.0001$], and a significant interaction [$F(3,76) = 167.603$, $p < 0.0001$] (Fig. 2C). At baseline, the C/I ratios were reduced in MD groups versus the NC+Sham group (all $p < 0.0001$. Fig. 2A,C), indicating that the MD model induced visual impairment. This impairment was reversed by rTMS: the MD group C/I values increased after rTMS (0.600 ± 0.142 to 1.254 ± 0.152, $p < 0.001$), but were not significantly different after sham stimulation (0.575 ± 0.167 to 0.645 ± 0.075, $p = 0.064$). However, in the normal groups (NC+sham and NC+rTMS), the C/I ratios were not significantly changed (Fig. 2C). Additionally, after intervention, the C/I values in the MD+rTMS group were markedly higher than in the MD+sham group ($p < 0.001$), but not significantly different from the NC+sham group ($p = 0.400$). These results suggest that 20 Hz rTMS promotes the recovery of an abnormal OD distribution in MD rats.

The detection of functional status of neurons in the left V1 region of rats using Nissl staining (Fig. 2B). In the NC+sham group, cortical neurons exhibited regular, dense arrangements with intact cellular structures and distinct boundaries. In contrast, the MD+sham group exhibited scattered cortical neuron arrangements, with cell body atrophy and indistinct nucleoli. Following rTMS stimulation, neuronal morphology improved in the MD group, while no obvious alterations were found for the NC group. Quantification of Nissl-positive cells showed a significant decrease in the MD+sham group when compared to the NC+sham group (110.625 ± 5.647 vs. 135.687 ± 3.009, $p < 0.001$). However, cell counts in the MD+rTMS group (127.687 ± 7.162) recovered to become not significantly different from the NC+sham group ($p > 0.05$, Fig. 2D).

Table 1. Primer sequences for the target genes in this study.

Gene	Forward (5′-3′)	Reverse (5′-3′)
PSD-95	GGTGAATGGAACAGAGGGGG	GATGGATCACGATCCGCCTT
BDNF	CTTGGAGAAGGAAACCGCCT	GTCCACACAAAGCTCTCGGA
NRF2	GCACATCCAGACAGACACCA	CTCTCAACGTGGCTGGGAAT
GPX4	ACGCCAAAGTCCTAGGAAGC	CTGCGAATTCGTGCATGGAG
FPN1	GGCACTTTGCAGTGTCTGTG	GTCACCAATGATGGCTCCCA
GAPDH	GAAGGTCGGTGTGAACGGAT	CCCATTTGATGTTAGCGGGAT
β-actin	AGATCAAGATCATTGCTCCTCCT	ACGCAGCTCAGTAACAGTCC

PSD-95, postsynaptic density protein 95; *BDNF*, brain-derived neurotrophic factor; *NRF2*, NF-E2-related factor 2; *GPX4*, glutathione peroxidase-4; *FPN1*, ferroportin-1; *GAPDH*, glyceraldehyde-3-phosphate dehydrogenase.

No significant change was induced by rTMS in NC rats in the NC+rTMS group (136.937 ± 7.600). Such observations suggest that 20 Hz rTMS may ameliorate MD-induced functional impairment in visual cortex neurons.

3.2 High-Frequency rTMS Improves Synaptic Structure and Functional Plasticity in the Visual Cortex of MD Rats

TEM was employed to assess alterations in synaptic ultrastructure within the left V1 induced by rTMS in MD rats (Fig. 3A). Two-way ANOVA revealed that MD significantly reduced synaptic density ($F(1,12) = 31.044$, $p < 0.001$), widened synaptic cleft width ($F(1,12) = 60.832$, $p < 0.001$), and shortened PSD length ($F(1,12) = 19.090$, $p = 0.001$). Meanwhile, the rTMS treatment also demonstrated significant main effects on the aforementioned indicators, including synaptic density ($F(1,12) = 7.143$, $p = 0.020$), PSD length ($F(1,12) = 15.381$, $p = 0.002$), and synaptic cleft width ($F(1,12) = 20.389$, $p = 0.001$). Bonferroni post-hoc analysis revealed that rTMS specifically ameliorated synaptic structural damage induced by MD: It significantly reduced synaptic cleft width ($p = 0.001$) and increased PSD length ($p = 0.013$) in the amblyopic model. Regarding synaptic density, the difference between the two groups was not statistically significant ($p = 0.180$, Fig. 3B–D), but the MD+rTMS group showed an upward trend.

PSD-95 and BDNF are two crucial synaptic function proteins in the brain. Therefore, this study further employed Western blotting to detect the abundance of these two proteins in rat visual cortex (Fig. 3E,F). For all original Western blotting figures of Fig. 3E,F, see **Supplementary Material**. Results revealed significant main effects of MD on both PSD-95 and BDNF expression (PSD-95: $F(1,12) = 23.033$, $p < 0.001$; BDNF: $F(1,12) = 12.253$, $p = 0.004$). Post hoc comparisons revealed that the effects of rTMS treatment were state-dependent. In the NC group, rTMS treatment did not significantly alter PSD-95 or BDNF expression levels. However, in the MD group, rTMS treatment significantly increased PSD-95 and BDNF expression ($p = 0.016$, $p = 0.041$, respectively), restoring both to near-normal levels (Fig. 3G,H). RT-qPCR analysis results were consistent with the trends observed above (Fig. 3I,J). This indicates that high-frequency rTMS may promote synaptic stability and plasticity by specifically modulating the expression of PSD-95 and BDNF.

3.3 High-Frequency rTMS Attenuates Oxidative Stress in the Visual Cortex of MD Rats

Given previous evidence that rTMS has antioxidant properties in addition to synaptic modulation, oxidative stress levels were assessed in the left V1. DHE staining showed ROS fluorescence intensity was significantly elevated in the MD+sham group relative to the NC+sham group (127.487 ± 6.886 vs. 98.792 ± 7.865, $p < 0.001$). Following rTMS intervention, ROS fluorescence intensity in the MD group markedly decreased (MD+rTMS: 112.453 ± 4.150, $p < 0.05$), to become not significantly different from NC+sham levels ($p > 0.05$) (Fig. 4A,B). Consistent with this, biochemical assay results demonstrated that MDA levels were significantly elevated in the MD+sham group relative to the NC+sham group (2.287 ± 0.210 μmol/gprot vs. 1.011 ± 0.129 μmol/gprot, $p < 0.0001$), while GSH content significantly decreased (2.214 ± 0.246 μmol/gprot vs. 4.676 ± 0.317 μmol/gprot, $p < 0.0001$). Following rTMS intervention, the MDA levels in the MD group were significantly reduced (MD+rTMS: 1.249 ± 0.118 μmol/gprot, $p < 0.0001$) and increased GSH content (MD+rTMS: 4.027 ± 0.116 μmol/gprot, $p < 0.0001$) (Fig. 4C,D). Furthermore, no significant differences were observed between the NC+rTMS and NC+sham groups for any parameters (NC+rTMS: ROS: 101.663 ± 7.137; MDA: 0.934 ± 0.052 μmol/gprot, GSH: 4.691 ± 0.270 μmol/gprot, all $p > 0.05$) (Fig. 4B–D). These results indicate that 20 Hz rTMS intervention is associated with the improvement of oxidative stress status in the visual cortex of MD rats.

3.4 High-Frequency rTMS Upregulates the Expression of NRF2/GPX4 in the Visual Cortex of MD Rats

Accumulating evidence has shown that rTMS modulates the NRF2/GPX4 pathway, which underlies its antioxidant and neuroprotective properties. Therefore, this research further examined the levels of NRF2/GPX4 path-

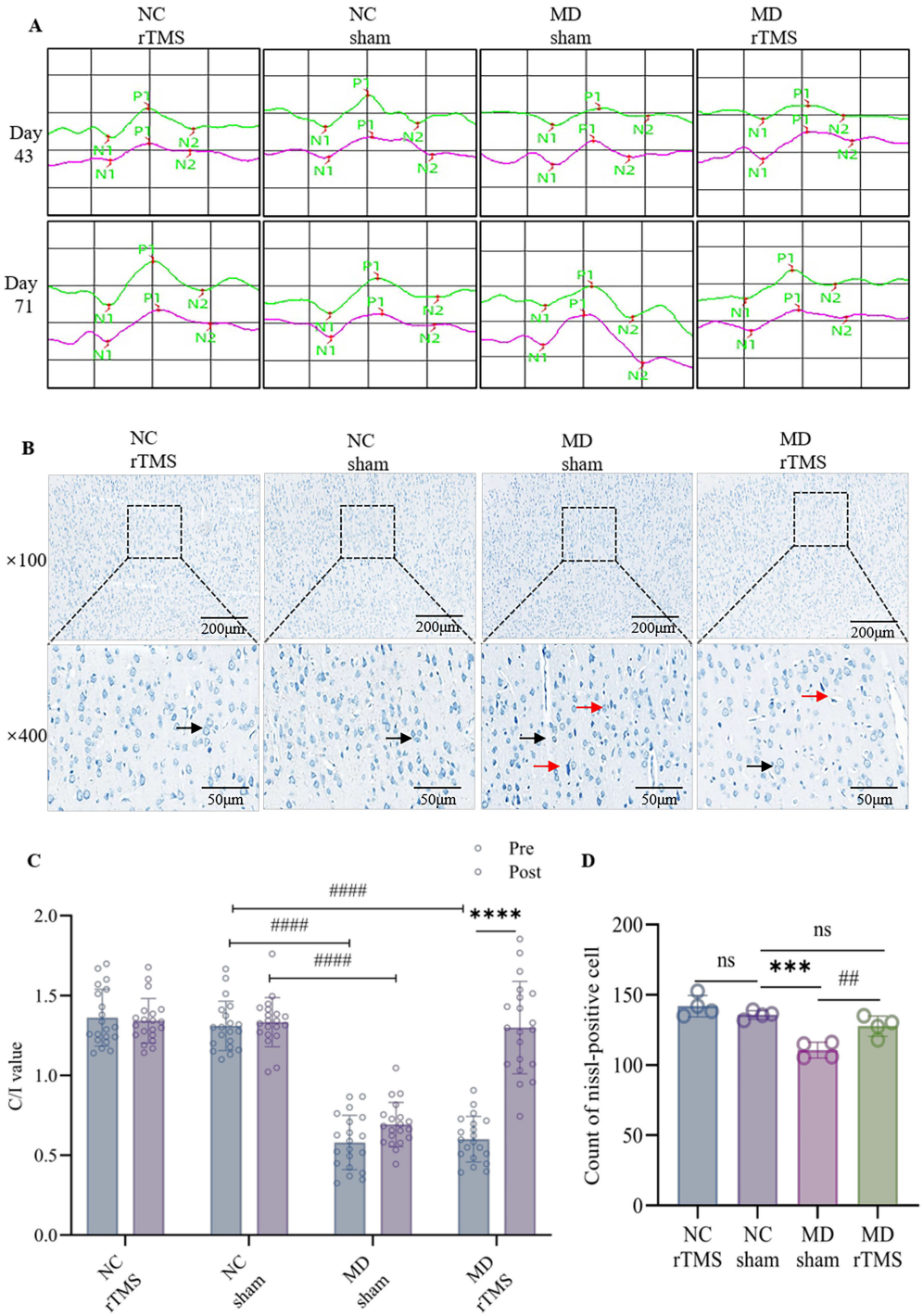

Fig. 2. High-frequency rTMS affects OD distribution and neuronal function in MD rats. (A) F-VEP waveforms before and after rTMS intervention in each group (n = 20); green: right eye; purple: left eye. (B) Histopathological changes in the left V1 observed via Nissl staining (n = 4); normal neurons (black arrows), Nissl-positive cells (red arrows); Scale bars: 200 μm and 50 μm. (C) Analysis of P1 wave amplitude in F-VEP across groups before and after rTMS intervention, expressed as C/I values (n = 20). Data were expressed as mean ± SD. $^{\#\#\#\#}$ indicates statistically significant difference between MD and NC+Sham groups, $p < 0.0001$; **** indicates statistically significant difference in MD+rTMS group before and after rTMS intervention, $p < 0.0001$. (D) Analysis of Nissl-positive cell counts across groups (n = 4). ^{ns} $p > 0.05$, *** $p < 0.001$ vs. NC+sham group; $^{\#\#}$ $p < 0.01$ vs. MD+sham group. rTMS, Repetitive transcranial magnetic stimulation; OD, ocular dominance; F-VEP, flash visual evoked potentials; SD, standard deviation; NC+sham, NC+sham stimulation.

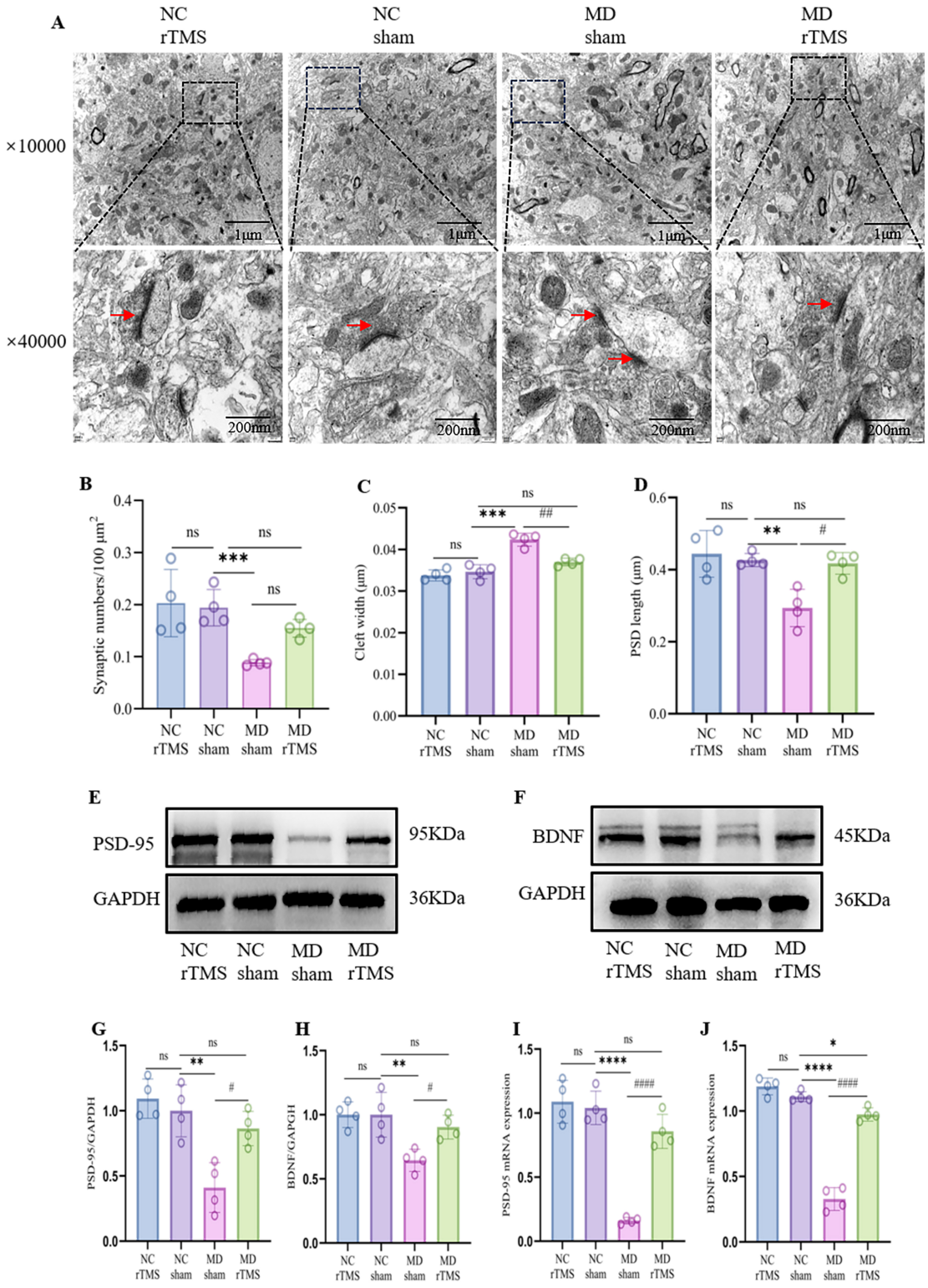

Fig. 3. High-frequency rTMS improves synaptic structure and plasticity in the visual cortex of MD rats. (A) TEM observation of synaptic ultrastructure in left V1 across groups (n = 4) (red arrows indicate synapses); Scale bars: 1 μm and 200 nm. (B) Synaptic number analysis (n = 4). (C) Synaptic cleft width analysis (n = 4). (D) Synaptic PSD length analysis (n = 4). (E,F) Western blotting detection of PSD-95 and BDNF protein expression across groups. (G–J) Differences in PSD-95 and BDNF protein levels and mRNA content among groups (n = 4), with GAPDH as the internal control protein. Data were expressed as mean ± SD. $^{ns}\ p > 0.05$, $^{*}\ p < 0.05$, $^{**}\ p < 0.01$, $^{***}\ p < 0.001$, $^{****}\ p < 0.0001$ vs. NC+sham group; $^{\#}\ p < 0.05$, $^{\#\#}\ p < 0.01$, $^{\#\#\#\#}\ p < 0.0001$ vs. MD+sham group. TEM, transmission electron microscopy; PSD-95, postsynaptic density protein 95; BDNF, brain-derived neurotrophic factor.

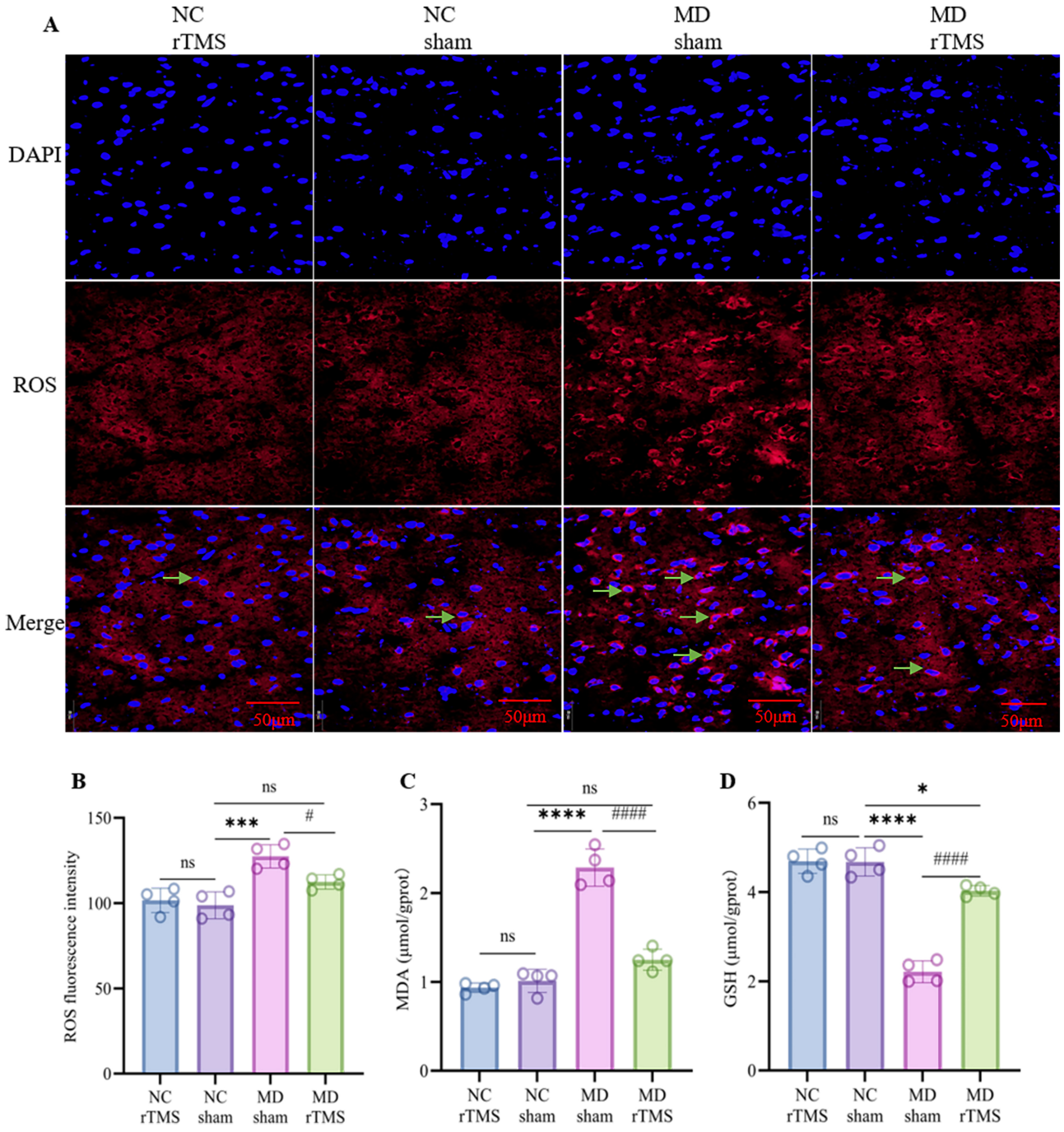

Fig. 4. High-frequency rTMS attenuates oxidative stress in the visual cortex of MD rats. (A) DHE staining detected ROS levels in the left V1 of each group (n = 4) (ROS marked with red fluorescence, nuclei labeled by DAPI, merged image indicated by green arrows). Scale bar: 50 μm. (B) ROS fluorescence intensity analysis (n = 4). (C) MDA content analysis (n = 4). (D) GSH content analysis (n = 4). Data were expressed as mean ± SD. ^{ns} $p > 0.05$, * $p < 0.05$, *** $p < 0.001$, **** $p < 0.0001$ vs. NC+sham group; $^{\#}$ $p < 0.05$, $^{\#\#\#\#}$ $p < 0.0001$ vs. MD+sham group. ROS, reactive oxygen species; DAPI, 4′,6-diamidino-2-phenylindole; MDA, malondialdehyde; GSH, glutathione.

way proteins and mRNA in the left visual cortex of rats across all groups (Fig. 5A,B). For all original Western blotting figures of Fig. 5A,B, see **Supplementary Material**. Results revealed a significant main effect of MD on NRF2 and GPX4 expression (NRF2: $F(1,12) = 26.166$, $p < 0.001$; GPX4: $F(1,12) = 54.334$, $p < 0.001$). Further comparisons revealed that protein expression levels of NRF2 and GPX4 were markedly reduced in the MD+sham group relative to the NC+sham group ($p < 0.001$). Conversely, following rTMS treatment, NRF2 and GPX4 protein levels were sig-

nificantly elevated in the MD+rTMS group compared to the MD+sham group ($p < 0.01$). No significant differences in protein expression were observed between the NC+rTMS and NC+sham groups (Fig. 5C,D). Similarly, qRT-PCR results revealed a significant downregulation of *NRF2* and *GPX4* mRNA expression in the MD+sham group relative to the NC+sham group ($p < 0.0001$). rTMS intervention significantly upregulated mRNA levels of these genes ($p < 0.001$), though they remained below NC+sham group levels (Fig. 5E,F). These results suggest that 20 Hz rTMS intervention is associated with upregulation of NRF2/GPX4 expression in the visual cortex of MD rats.

3.5 High-Frequency rTMS Reduces Iron Accumulation in the Visual Cortex of MD Rats and Improves Iron Metabolism

Research indicates that the NRF2/GPX4 pathway plays an important role in regulating iron homeostasis. To investigate whether iron metabolism imbalance is related to amblyopia formation and whether high-frequency rTMS intervention involves iron metabolism regulation, Enhanced Prussian blue iron staining was used to assess iron deposition in the left V1 of rats (Fig. 6A). Results showed that both the NC+rTMS and NC+sham groups exhibited lighter iron staining, while the MD+sham group demonstrated significantly increased iron deposition. rTMS intervention visibly reduced this pathological iron accumulation in MD rats, although some deposition remained. Consistent with the staining results, biochemical quantification of Fe^{2+} content confirmed a significant increase in the MD+sham group compared to the NC+sham group (203.273 $\pm$ 25.604 vs. 105.008 $\pm$ 8.402 µmol/kg wet weight, $p < 0.0001$). However, rTMS effectively reduced Fe^{2+} levels (MD+rTMS: 140.389 $\pm$ 11.899 µmol/kg wet weight, $p = 0.001$), bringing them close to the NC+sham group ($p = 0.041$) (Fig. 6B). Furthermore, rTMS did not significantly alter Fe^{2+} levels in NC rats (NC+rTMS: 102.693 $\pm$ 8.451 µmol/kg wet weight, $p > 0.05$).

Western blotting and qRT-PCR were employed to further assess FPN1 expression levels (Fig. 6C). For all original Western blotting figures of Fig. 6C, see **Supplementary Material**. Results revealed significantly reduced FPN1 expression in the MD+sham group in comparison with the NC+sham group ($p < 0.0001$), whereas rTMS intervention significantly upregulated its expression (MD+rTMS vs. MD+sham, $p < 0.001$; vs. NC+sham, $p = 0.073$). Furthermore, there was no notable difference in FPN1 expression between the NC+rTMS and NC+sham groups (Fig. 6D,E). These findings indicate that 20 Hz rTMS intervention was associated with reduced MD-induced iron accumulation, modulated FPN1 expression, and improved iron metabolism.

4. Discussion

This study demonstrates that high-frequency rTMS effectively ameliorates abnormal OD and promotes the recovery of synaptic structure and functional plasticity in the visual cortex of MD amblyopic rats. Specifically, rTMS intervention significantly increased the C/I values in MD rats, upregulated the expression of PSD-95 and BDNF, facilitated synapse remodeling, and enhanced synapse density. Further investigations revealed that high-frequency rTMS upregulates the expression of NRF2/GPX4 pathway-related proteins in the visual cortex of MD rats, which is associated with the alleviation of oxidative stress and the improvement of iron metabolism. This reveals a previously unreported association, which deepens the understanding of rTMS by providing new insights and theoretical support for the treatment and pathogenesis of amblyopia.

Recently, rTMS has emerged as a novel therapeutic strategy for adult amblyopia, with its efficacy closely correlated to stimulation parameters, among which stimulation intensity and frequency are critical factors [23,24]. For example, in an *in vitro* hippocampal neuron model, magnetic stimulation at 40%–60% of maximum output intensity enhanced neuronal survival rates and ferrous enzyme expression, whereas 100% intensity resulted in decreased survival rates and suppressed enzyme expression [19]. Similar studies indicate that high-frequency rTMS at 33% of maximum output intensity significantly improves neurological and cortical damage in rats with artery occlusion by inhibiting ferroptosis and inflammatory responses [25]. Furthermore, varying stimulation frequencies and treatment durations yield distinct outcomes. High-frequency rTMS (20 Hz) exerts long-term effects on neuroplasticity markers (such as BDNF and glutamate receptor 1), while low-frequency stimulation (1 Hz) has no significant long-term effect [26]. A single 20-minute rTMS treatment does not alter gamma-aminobutyric acid (GABA) or glutamate concentrations in the visual cortex. By contrast, five daily rTMS treatments significantly reduce GABA levels in the visual cortex, and this effect persists for at least 24 hours [27]. Similarly, a study in SAMP8 mice demonstrated that 25 Hz high-frequency rTMS improved spatial learning and memory abilities, with 28 consecutive days of stimulation showing superior effects when compared to 14 days [18]. However, current rTMS studies in amblyopia remain largely confined to short-term efficacy observations, and optimal stimulation parameters remain undefined. Therefore, building upon prior work, this study employed 20 Hz rTMS at 30% of the maximum output intensity for 28 days in MD rats to evaluate its long-term therapeutic potential. Additionally, a sham-stimulation control group was established in the experiment by increasing the distance between the coil and the rat's head to exclude the influence of nonspecific effects such as sound and thermal stimulation. However, it is still difficult to fully simulate the somatosensory and vibration cues during real stimulation.

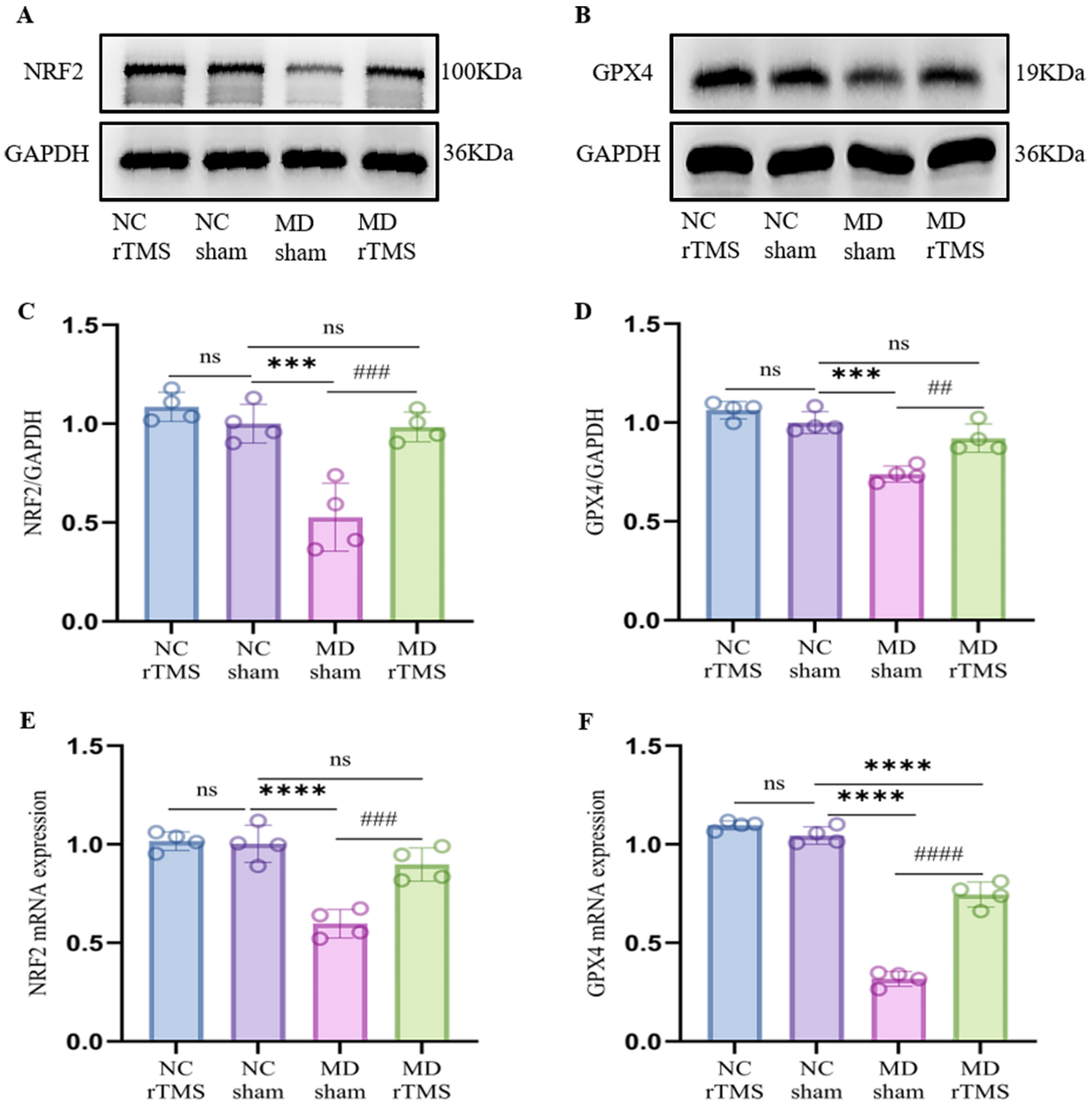

Fig. 5. High-frequency rTMS upregulates the expression of NRF2/GPX4 in the visual cortex of MD rats. (A,B) Western blotting detected protein expression of NRF2 and GPX4 in the left visual cortex across groups (n = 4). (C,D) Comparisons of NRF2 and GPX4 protein expression across groups. (E,F) Differences in *NRF2* and *GPX4* mRNA contents among groups (n = 4). GAPDH was used as the internal control protein. Data were expressed as mean ± SD. ^{ns} $p > 0.05$, *** $p < 0.001$, **** $p < 0.0001$ vs. NC+sham group; $^{\#\#}$ $p < 0.01$, $^{\#\#\#}$ $p < 0.001$, $^{\#\#\#\#}$ $p < 0.0001$ vs. MD+sham group. NRF2/GPX4, NF-E2-related factor 2/glutathione peroxidase-4.

The visual cortex, as the higher-level center for visual information processing, exhibits structural and functional alterations closely associated with the occurrence and development of amblyopia [28]. During the critical period of visual development, suturing one eye shut in animals induces changes in OD within cortical neurons—a phenomenon termed ocular dominance plasticity (ODP) [22]. F-VEP serves as an objective method for evaluating visual function, reflecting the signal conduction status from retina to visual cortex and changes in ODP [29]. The variation in its C/I ratio is widely recognized as a reliable electrophysiological indicator of cortical OD column shift or rebalancing. This study demonstrated that the C/I values in MD rats were significantly lower than the NC group. This indicates that either diminished information was sent from the deprived eye to the visual cortex, or that increased information was sent from the non-deprived eye. Following rTMS, the C/I values in MD rats approached normal levels, suggesting restoration of ODP in the visual cortex, consistent with previous findings [30,31]. Synapses serve as the fundamental

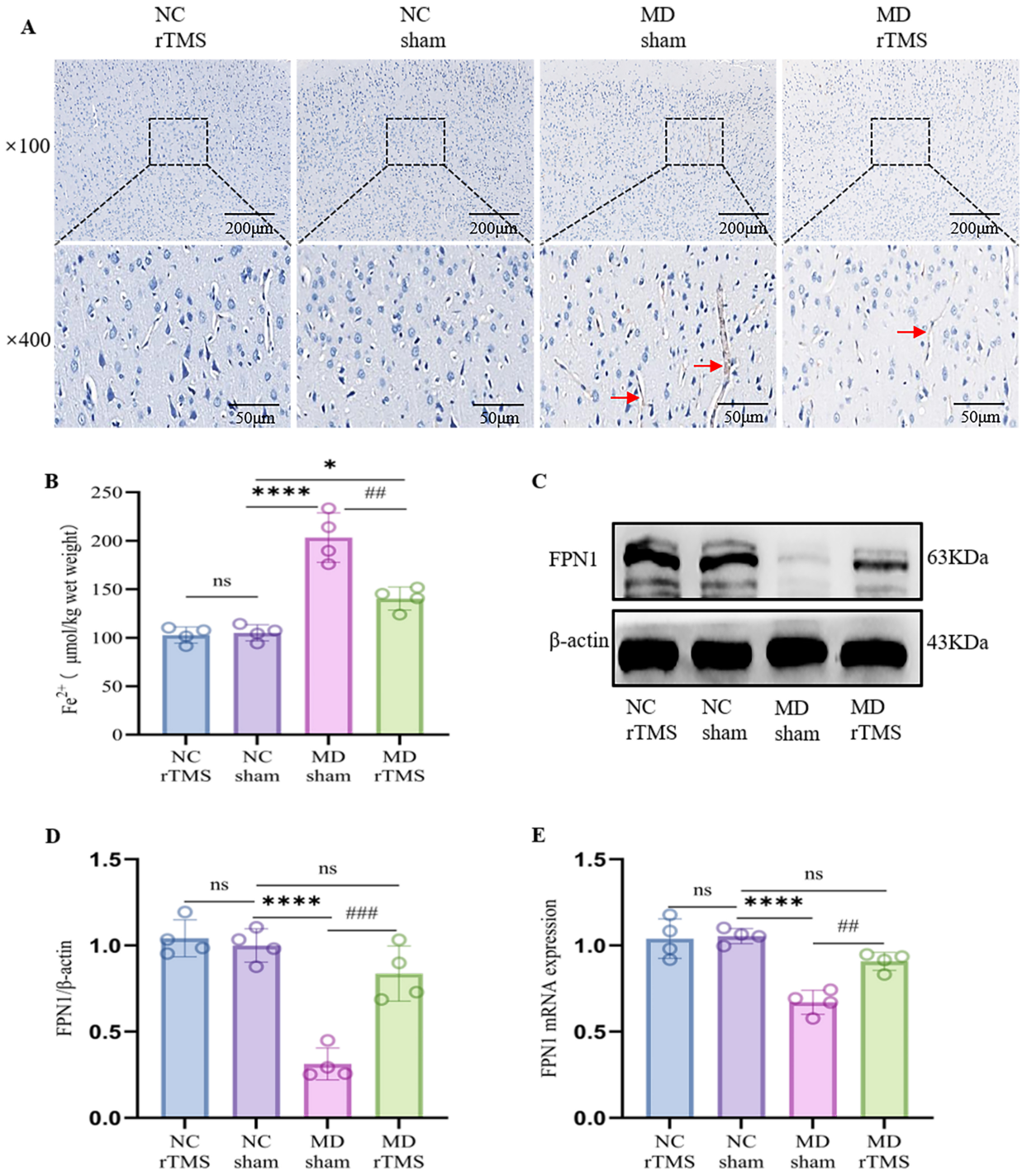

Fig. 6. High-frequency rTMS reduces iron accumulation in the visual cortex of MD rats and improves iron metabolism. (A) Enhanced Prussian blue iron staining to detect iron deposition in the left V1 of each group (n = 4) (iron staining particles are indicated by red arrows); scale: 200 μm and 50 μm. (B) Fe^{2+} content variation (n = 4). (C) Western blotting detection of FPN1 protein expression (n = 4). (D) Differences in FPN1 protein levels among groups. (E) Differences in *FPN1* mRNA content among groups (n = 4). *β*-actin served as the endogenous reference protein. Data were presented as mean ± SD. ^{ns} $p > 0.05$, * $p < 0.05$, **** $p < 0.0001$ vs. NC+sham group; $^{\#\#}$ $p < 0.01$, $^{\#\#\#}$ $p < 0.001$ vs. MD+sham group. FPN1, ferroportin-1.

units for inter-neuronal communication and form the critical foundation for the structural and functional development of visual cortex neurons [32]. Extensive prior research has demonstrated that MD disrupts synaptic structures in visual cortex neurons and reduces PSD-95 and BDNF expression levels [1]. These latter two proteins are critical for intracellular signal transmission, ion channel modulation, synaptic transmission, and neuronal excitability [33]. Similarly, this

study found that rats in the MD group exhibited reduced synaptic numbers and increased synaptic cleft widths in the visual cortex. Following rTMS intervention, these structural parameters showed marked improvement, accompanied by significant upregulation of PSD-95 and BDNF expression levels. This indicates that high-frequency rTMS effectively improves the ODP in MD-induced amblyopic rats by promoting the recovery of synaptic structural and functional plasticity in the visual cortex.

In addition to the regulation of synaptic plasticity, rTMS has also been reported to mitigate oxidative damage [34]. Oxidative stress refers to a state in which the accumulation of ROS and reactive nitrogen species exceeds the antioxidant defense capacity of the body, resulting in cellular damage [35]. Studies indicate that rTMS mitigates neuronal oxidative damage by scavenging ROS or activating endogenous antioxidant systems [36]. Recent studies indicate that damage and loss of visual cortex neurons constitute common pathological alterations in amblyopia [37], though few investigations have explored whether this correlates with oxidative stress responses. This study detected significantly elevated ROS and MDA levels alongside markedly reduced GSH content in the visual cortex of MD rats, suggesting pronounced oxidative stress damage in their visual cortex. Following high-frequency rTMS treatment, ROS and MDA levels decreased while GSH content increased, suggesting high-frequency rTMS effectively attenuates cortical oxidative stress. A previous study reported that while antioxidant supplementation (vitamins E and C) counteracts oxidative stress, it also interferes with the promotion of visual cortex plasticity by exercise in amblyopic rats [38]. This contrasts with findings of the present study, where high-frequency rTMS was associated with improved synaptic plasticity functions despite concurrent modulation of oxidative stress, suggesting a complex relationship between oxidative stress and neural plasticity. rTMS may enhance neural plasticity while providing antioxidant effects through more precise regulatory mechanisms. Nevertheless, the specific molecular mechanisms underlying MD-induced oxidative stress and its regulation by high-frequency rTMS warrant further investigation.

Studies have shown that the NRF2/GPX4 pathway is a critical endogenous antioxidant pathway associated with various neurological disorders [39]. NRF2 activity is influenced by neuronal metabolic status [40]. Its downregulation leads to mitochondrial dysfunction, compromises neuronal energy supply, and impairs visual cortex plasticity [10,41], and closely correlates with the pathogenesis of amblyopia [42]. Furthermore, its downstream factor GPX4 utilizes GSH to reduce peroxides, thereby protecting cells from oxidative damage [43]. In this study, both NRF2 and GPX4 expression were significantly reduced in the visual cortex of MD rats, suggesting that the NRF2/GPX4 pathway may participate in oxidative stress-induced damage during amblyopia. The restoration of their expression following high-frequency rTMS intervention suggests that rTMS may enhance antioxidant activity in association with modulation of the NRF2/GPX4 pathway. This result is consistent with previous studies: TMS promotes nuclear translocation of NRF2 in a Huntington's disease-like rat and elevates the levels of GPx, catalase, and GSH [44]. High-frequency rTMS alleviates neuroinflammation and oxidative stress in vascular dementia rats by regulating the NRF2/GPX4 pathway, thereby enhancing cognitive function [17]. Collectively, these results suggest an association between high-frequency rTMS and antioxidant effects alongside improvement of visual cortex neuronal function.

Furthermore, multiple studies indicate that the NRF2/GPX4 pathway extends beyond antioxidant defense to include participation in maintaining iron homeostasis [45,46]. Iron participates in numerous biochemical reactions through its unique Fe^{2+}/Fe^{3+} redox properties, and its metabolic disorder can lead to serious consequences [47]. Iron deficiency affects neuronal maturation and myelination, whereas iron overload can induce lipid peroxidation and ferroptosis, leading to synaptic dysfunction and neuronal damage [48]. GPX4 has been identified as a core inhibitor of ferroptosis [49]. NRF2 suppresses ferroptosis by regulating the expression of iron metabolism-related genes [50]. Thus, an imbalance in the NRF2/GPX4 pathway may disrupt iron metabolism in the visual cortex of amblyopic rats. FPN1, the sole iron export protein in the body, plays a crucial role in iron homeostasis regulation, with its expression directly controlled by NRF2 [51]. Studies indicate that FPN1 expression is reduced in multiple organs of NRF2 knockout mice, accompanied by abnormal iron accumulation and elevated ROS levels [52]. Conversely, activating NRF2 upregulates FPN1, enhancing iron efflux capacity and effectively mitigating neurotoxic effects induced by iron overload [53]. This study found significantly reduced FPN1 expression and elevated Fe^{2+} levels in the MD rat visual cortex, suggesting that iron metabolism disorders may be involved in the pathological process of amblyopia. High-frequency rTMS intervention markedly upregulated FPN1 expression and reduced Fe^{2+} levels, suggesting that rTMS reduces abnormal iron accumulation in the visual cortex of MD rats and improves iron metabolism. This ameliorative effect may be closely associated with its regulation of the NRF2 signalling pathway. These findings provide novel correlational experimental evidence for the neural mechanisms underlying high-frequency rTMS treatment of amblyopia.

5. Limitation

However, this study has certain limitations. Firstly, the 80 mm diameter coil employed in this research is relatively large in relation to the size of a rat's head, potentially leading to magnetic field diffusion into neighbouring brain regions. Consequently, the observed effects may

not be strictly confined to the visual cortex; future studies require the use of smaller, more focused coils to validate their brain region specificity. Secondly, the study exclusively utilized the MD amblyopia model without exploring other amblyopia subtypes, leaving the generalizability of high-frequency rTMS mechanisms to be validated. Finally, this study only preliminarily explored the potential link between amblyopia development and the downregulation of the NRF2/GPX4 pathway alongside high-frequency rTMS intervention. However, the critical role of this pathway requires further clarification through experimental approaches such as gene knockout or specific pharmacological interventions in subsequent research.

6. Conclusions

This study demonstrates that high-frequency rTMS effectively promotes the restoration of abnormal OD in amblyopic rats. The therapeutic effects involve a multilevel synergistic process, whereby rTMS directly enhances synaptic plasticity in the visual cortex. Additionally, this study reveals that the neuroprotective effects of rTMS are closely associated with the upregulation of NRF2/GPX4 pathway protein expression, attenuated oxidative stress, and restored iron metabolism within the visual cortex of amblyopic rats.

Availability of Data and Materials

The datasets used and analyzed during the current study are available from the corresponding author on reasonable request.

Author Contributions

QLi: Conceptualization, Methodology, Investigation, Data Curation, Formal analysis, Visualization, Writing—Original Draft, Writing—Review & Editing. YY: Methodology, Investigation, Writing—Original Draft. QLu: Investigation, Data Curation, Formal analysis, Visualization, Writing—Review & Editing. YZ: Conceptualization, Resources, Funding acquisition, Supervision, Writing—Review & Editing. XY: Investigation, Resources, Writing—Review & Editing. HW and ZL: Methodology, Investigation, Writing—Review & Editing. WL: Data Curation, Visualization, Writing—Review & Editing. LW and WS: Conceptualization, Writing—Review & Editing. All authors read and approved the final manuscript. All authors have participated sufficiently in the work and agreed to be accountable for all aspects of the work.

Ethics Approval and Consent to Participate

This study was approved by the Animal Ethics Committee of North Sichuan Medical College (Approval No.: 2024016). The protocol followed the ARRIVE guidelines for animal use. All procedures were strictly performed in compliance with the National Institutes of Health Guide for the Care and Use of Laboratory Animals.

Acknowledgment

We would like to express our gratitude to all those who helped us during the writing of this manuscript.

Funding

This work was supported by Natural Science Foundation Project of Sichuan Provincial Science and Technology Department (2025ZNSFSC0270); Nanchong Science and Technology Bureau Project (22SXQT0350); Zhoukou Science and Technology Bureau Project (2024ptgg38).

Conflicts of Interest

The authors declare no conflicts of interest.

Supplementary Material

Supplementary material associated with this article can be found, in the online version, at https://doi.org/10.31083/JIN48602.

References

[1] Wang L, Ji Y, Mei H, Gong X, Miao H, Zhu Z, *et al*. Electroacupuncture improves V1 cortex synaptic plasticity via the CREB/BDNF/TrkB pathway in juvenile rats with monocular deprivation. Experimental Eye Research. 2025; 250: 110169. https://doi.org/10.1016/j.exer.2024.110169.

[2] Hu B, Liu Z, Zhao J, Zeng L, Hao G, Shui D, *et al*. The Global Prevalence of Amblyopia in Children: A Systematic Review and Meta-Analysis. Frontiers in Pediatrics. 2022; 10: 819998. https://doi.org/10.3389/fped.2022.819998.

[3] Mao D, Liu C, Yin Z, Cui Z, Zhang J, Li X, *et al*. Effects of anisometropic amblyopia on visual cognitive functions in children. Clinical & Experimental Ophthalmology. 2024; 53: 344–355. https://doi.org/10.1111/ceo.14472.

[4] Sterkin A, Yehezkel O. Binocular treatment of amblyopia: current state and recent advances. Current Opinion in Ophthalmology. 2025; 36: 237–246. https://doi.org/10.1097/ICU.0000000000001121.

[5] Tuna AR, Pinto N, Fernandes A, Brardo FM, Pato MV. Can repetitive transcranial magnetic stimulation influence the visual cortex of adults with amblyopia? - systematic review. Clinical & Experimental Optometry. 2024; 107: 691–697. https://doi.org/10.1080/08164622.2024.2363369.

[6] Zheng J, Zhang W, Liu L, Hung Yap MK. Low frequency repetitive transcranial magnetic stimulation promotes plasticity of the visual cortex in adult amblyopic rats. Frontiers in Neuroscience. 2023; 17: 1109735. https://doi.org/10.3389/fnins.2023.1109735.

[7] Hess RF, Thompson B. New insights into amblyopia: binocular therapy and noninvasive brain stimulation. Journal of American Association for Pediatric Ophthalmology and Strabismus. 2013; 17: 89–93. https://doi.org/10.1016/j.jaapos.2012.10.018.

[8] Navarro E, Esteras N. Multitarget Effects of Nrf2 Signalling in the Brain: Common and Specific Functions in Different Cell Types. Antioxidants. 2024; 13: 1502. https://doi.org/10.3390/antiox13121502.

[9] Luchkova A, Mata A, Cadenas S. Nrf2 as a regulator of energy

metabolism and mitochondrial function. FEBS Letters. 2024; 598: 2092–2105. https://doi.org/10.1002/1873-3468.14993.

[10] Yu L, Yang SJ. AMP-activated protein kinase mediates activity-dependent regulation of peroxisome proliferator-activated receptor gamma coactivator-1alpha and nuclear respiratory factor 1 expression in rat visual cortical neurons. Neuroscience. 2010; 169: 23–38. https://doi.org/10.1016/j.neuroscience.2010.04.063.

[11] Zeng T, Li J, Xie L, Dong Z, Chen Q, Huang S, *et al*. Nrf2 regulates iron-dependent hippocampal synapses and functional connectivity damage in depression. Journal of Neuroinflammation. 2023; 20: 212. https://doi.org/10.1186/s12974-023-02875-x.

[12] Wei C. The role of glutathione peroxidase 4 in neuronal ferroptosis and its therapeutic potential in ischemic and hemorrhagic stroke. Brain Research Bulletin. 2024; 217: 111065. https://doi.org/10.1016/j.brainresbull.2024.111065.

[13] Zhou A, Feng HY, Fan CN, Wang J, Yuan ZY, Xu GH, *et al*. Asiaticoside Attenuates Chronic Restraint Stress-Induced Hippocampal CA1 Neuronal Ferroptosis via Activating BDNF/Nrf2/GPX4 Signaling Pathway. Drug Design, Development and Therapy. 2025; 19: 793–810. https://doi.org/10.2147/DDDT.S509208.

[14] Zhou J, Zhang H, Wang Y, Huang Q. The Nrf2-GPX4 axis mitigates ferroptosis-driven early brain injury in experimental subarachnoid hemorrhage. Brain Research. 2025; 1863: 149761. https://doi.org/10.1016/j.brainres.2025.149761.

[15] Gao Q, Zhou Y, Chen Y, Hu W, Jin W, Zhou C, *et al*. Role of iron in brain development, aging, and neurodegenerative diseases. Annals of Medicine. 2025; 57: 2472871. https://doi.org/10.1080/07853890.2025.2472871.

[16] Yehia A, Melhuish Beaupre LM, Ho MC, Biernnacka JM, Frye MA, Abulseoud OA. Ferroptosis as a potential molecular mechanism of bipolar disorder. Translational Psychiatry. 2025; 15: 205. https://doi.org/10.1038/s41398-025-03429-w.

[17] Jin WJ, Zhu XX, Luo KT, Wang S, Li JA, Qian LF, *et al*. Enhancement of Cognitive Function in Rats with Vascular Dementia Through Modulation of the Nrf2/GPx4 Signaling Pathway by High-Frequency Repetitive Transcranial Magnetic Stimulation. Physiological Research. 2024; 73: 857–868. https://doi.org/10.33549/physiolres.935330.

[18] Xu Y, Xu M, Zhou C, Sun L, Cai W, Li X. Ferroptosis and its implications in treating cognitive impairment caused by aging: A study on the mechanism of repetitive transcranial magnetic stimulation. Experimental Gerontology. 2024; 192: 112443. https://doi.org/10.1016/j.exger.2024.112443.

[19] Wang Y, Fang K, He S, Fan Y, Yu J, Zhang X. Effects of repetitive magnetic stimulation on the growth of primarily cultured hippocampus neurons in vitro and their expression of iron-containing enzymes. Neuropsychiatric Disease and Treatment. 2019; 15: 927–934. https://doi.org/10.2147/NDT.S199328.

[20] Castillo-Padilla DV, Funke K. Effects of chronic iTBS-rTMS and enriched environment on visual cortex early critical period and visual pattern discrimination in dark-reared rats. Developmental Neurobiology. 2016; 76: 19–33. https://doi.org/10.1002/dneu.22296.

[21] Khazipov R, Zaynutdinova D, Ogievetsky E, Valeeva G, Mitrukhina O, Manent JB, *et al*. Atlas of the Postnatal Rat Brain in Stereotaxic Coordinates. Frontiers in Neuroanatomy. 2015; 9: 161. https://doi.org/10.3389/fnana.2015.00161.

[22] Chen K, Zhao Y, Liu T, Su Z, Yu H, Chan LLH, *et al*. Monocular Visual Deprivation and Ocular Dominance Plasticity Measurement in the Mouse Primary Visual Cortex. Journal of Visualized Experiments: JoVE. 2020; 10.3791/60600. https://doi.org/10.3791/60600.

[23] Park AS, Thompson B. Non-invasive brain stimulation and vision rehabilitation: a clinical perspective. Clinical & Experimental Optometry. 2024; 107: 594–602. https://doi.org/10.1080/08164622.2024.2349565.

[24] Lin Y, Cai K. Transcranial magnetic stimulation-based neuroplasticity in the treatment of amblyopia. Journal of Neuroscience Methods. 2025; 419: 110464. https://doi.org/10.1016/j.jneumeth.2025.110464.

[25] Zhou GJ, Liu DN, Huang XR, Wu Q, Feng WB, Zeng YH, *et al*. High-frequency repetitive transcranial magnetic stimulation protects against cerebral ischemia/reperfusion injury in rats: Involving the mitigation of ferroptosis and inflammation. Brain and Behavior. 2023; 13: e2988. https://doi.org/10.1002/brb3.2988.

[26] Gersner R, Kravetz E, Feil J, Pell G, Zangen A. Long-term effects of repetitive transcranial magnetic stimulation on markers for neuroplasticity: differential outcomes in anesthetized and awake animals. The Journal of Neuroscience. 2011; 31: 7521–7526. https://doi.org/10.1523/JNEUROSCI.6751-10.2011.

[27] Rafique SA, Steeves JKE. Assessing differential effects of single and accelerated low-frequency rTMS to the visual cortex on GABA and glutamate concentrations. Brain and Behavior. 2020; 10: e01845. https://doi.org/10.1002/brb3.1845.

[28] Nasr S, Skerswetat J, Gaier ED, Malladi SN, Kennedy B, Tootell RBH, *et al*. Differential Impacts of Strabismic and Anisometropic Amblyopia on the Mesoscale Functional Organization of the Human Visual Cortex. The Journal of Neuroscience. 2025; 45: e0745242024. https://doi.org/10.1523/JNEUROSCI.0745-24.2024.

[29] Gavornik JP, Bear MF. The visual evoked potential is a sensitive and powerful measure of experience-dependent visual cortical plasticity in mice. Current Opinion in Neurobiology. 2025; 93: 103019. https://doi.org/10.1016/j.conb.2025.103019.

[30] Thompson B, Mansouri B, Koski L, Hess RF. Brain plasticity in the adult: modulation of function in amblyopia with rTMS. Current Biology: CB. 2008; 18: 1067–1071. https://doi.org/10.1016/j.cub.2008.06.052.

[31] Tuna AR, Pinto N, Brardo FM, Fernandes A, Nunes AF, Pato MV. Transcranial Magnetic Stimulation in Adults With Amblyopia. Journal of Neuro-ophthalmology. 2020; 40: 185–192. https://doi.org/10.1097/WNO.0000000000000828.

[32] Thomas CI, Ryan MA, McNabb MC, Kamasawa N, Scholl B. Astrocyte coverage of excitatory synapses correlates to measures of synapse structure and function in ferret primary visual cortex. Glia. 2024; 72: 1785–1800. https://doi.org/10.1002/glia.24582.

[33] De Luca P, Mele M, Tanqueiro S, Napoli F, Butkevičiūtė U, Souto AC, *et al*. Synaptic accumulation of GluN2B-containing NMDA receptors mediates the effects of BDNF-TrkB signalling on synaptic plasticity and in hyperexcitability during status epilepticus. Journal of Biomedical Science. 2025; 32: 82. https://doi.org/10.1186/s12929-025-01164-4.

[34] Medina-Fernández FJ, Escribano BM, Padilla-Del-Campo C, Drucker-Colín R, Pascual-Leone Á, Túnez I. Transcranial magnetic stimulation as an antioxidant. Free Radical Research. 2018; 52: 381–389. https://doi.org/10.1080/10715762.2018.1434313.

[35] Saputra F, Kishida M, Hu SY. Oxidative stress induced by hydrogen peroxide disrupts zebrafish visual development by altering apoptosis, antioxidant and estrogen related genes. Scientific Reports. 2024; 14: 14454. https://doi.org/10.1038/s41598-024-64933-5.

[36] Velioglu HA, Hanoglu L, Bayraktaroglu Z, Toprak G, Guler EM, Bektay MY, *et al*. Left lateral parietal rTMS improves cognition and modulates resting brain connectivity in patients with Alzheimer's disease: Possible role of BDNF and oxidative stress. Neurobiology of Learning and Memory. 2021; 180: 107410. https://doi.org/10.1016/j.nlm.2021.107410.

[37] Acar K, Kiorpes L, Movshon JA, Smith MA. Altered func-

tional interactions between neurons in primary visual cortex of macaque monkeys with experimental amblyopia. Journal of Neurophysiology. 2019; 122: 2243–2258. https://doi.org/10.1152/jn.00232.2019.

[38] Sansevero G, Consorti A, Di Marco I, Terzibasi Tozzini E, Cellerino A, Sale A. Antioxidants Prevent the Effects of Physical Exercise on Visual Cortical Plasticity. Cells. 2022; 12: 48. https://doi.org/10.3390/cells12010048.

[39] Yang S, Wang L, Zeng Y, Wang Y, Pei T, Xie Z, *et al*. Salidroside alleviates cognitive impairment by inhibiting ferroptosis via activation of the Nrf2/GPX4 axis in SAMP8 mice. Phytomedicine. 2023; 114: 154762. https://doi.org/10.1016/j.phymed.2023.154762.

[40] Wong-Riley MTT, Yang SJ, Liang HL, Ning G, Jacobs P. Quantitative immuno-electron microscopic analysis of nuclear respiratory factor 2 alpha and beta subunits: Normal distribution and activity-dependent regulation in mammalian visual cortex. Visual Neuroscience. 2005; 22: 1–18. https://doi.org/10.1017/S0952523805221016.

[41] Esteras N, Abramov AY. Nrf2 as a regulator of mitochondrial function: Energy metabolism and beyond. Free Radical Biology & Medicine. 2022; 189: 136–153. https://doi.org/10.1016/j.freeradbiomed.2022.07.013.

[42] Xie J, Luo Y, Wei L, Fan H, Wang Y, Wang Q, *et al*. Effects of environmental enrichment on GLUT expression in the visual cortex of amblyopic rats. Brain Research. 2024; 1836: 148933. https://doi.org/10.1016/j.brainres.2024.148933.

[43] Liu Y, Wan Y, Jiang Y, Zhang L, Cheng W. GPX4: The hub of lipid oxidation, ferroptosis, disease and treatment. Biochimica et Biophysica Acta. Reviews on Cancer. 2023; 1878: 188890. https://doi.org/10.1016/j.bbcan.2023.188890.

[44] Tasset I, Pérez-Herrera A, Medina FJ, Arias-Carrión O, Drucker-Colín R, Túnez I. Extremely low-frequency electromagnetic fields activate the antioxidant pathway Nrf2 in a Huntington's disease-like rat model. Brain Stimulation. 2013; 6: 84–86. https://doi.org/10.1016/j.brs.2012.03.015.

[45] Mohan M, Mannan A, Kakkar C, Singh TG. Nrf2 and Ferroptosis: Exploring Translational Avenues for Therapeutic Approaches to Neurological Diseases. Current Drug Targets. 2025; 26: 33–58. https://doi.org/10.2174/0113894501320839240918110656.

[46] Chen J, Yin C, Zhang Y, Lai X, Liu C, Luo Y, *et al*. EGCG Alleviates DSS-Induced Colitis by Inhibiting Ferroptosis Through the Activation of the Nrf2-GPX4 Pathway and Enhancing Iron Metabolism. Nutrients. 2025; 17: 547. https://doi.org/10.3390/nu17030547.

[47] Gao G, You L, Zhang J, Chang YZ, Yu P. Brain Iron Metabolism, Redox Balance and Neurological Diseases. Antioxidants. 2023; 12: 1289. https://doi.org/10.3390/antiox12061289.

[48] Silvestri L, Pettinato M, Furiosi V, Bavuso Volpe L, Nai A, Pagani A. Managing the Dual Nature of Iron to Preserve Health. International Journal of Molecular Sciences. 2023; 24: 3995. https://doi.org/10.3390/ijms24043995.

[49] Zhang W, Liu Y, Liao Y, Zhu C, Zou Z. GPX4, ferroptosis, and diseases. Biomedicine & Pharmacotherapy. 2024; 174: 116512. https://doi.org/10.1016/j.biopha.2024.116512.

[50] Xiang Y, Song X, Long D. Ferroptosis regulation through Nrf2 and implications for neurodegenerative diseases. Archives of Toxicology. 2024; 98: 579–615. https://doi.org/10.1007/s00204-023-03660-8.

[51] Qian ZM, Li W, Guo Q. Ferroportin1 in the brain. Ageing Research Reviews. 2023; 88: 101961. https://doi.org/10.1016/j.arr.2023.101961.

[52] Liu Z, Han K, Huo X, Yan B, Gao M, Lv X, *et al*. Nrf2 knockout dysregulates iron metabolism and increases the hemolysis through ROS in aging mice. Life Sciences. 2020; 255: 117838. https://doi.org/10.1016/j.lfs.2020.117838.

[53] Tian H, Xiong Y, Zhang Y, Leng Y, Tao J, Li L, *et al*. Activation of NRF2/FPN1 pathway attenuates myocardial ischemia-reperfusion injury in diabetic rats by regulating iron homeostasis and ferroptosis. Cell Stress & Chaperones. 2022; 27: 149–164. https://doi.org/10.1007/s12192-022-01257-1.